Journal of Chemistry and Technologies, 2025, *33*(4), 948-957

Journal of Chemistry and Technologies

pISSN 2663-2934 (Print), ISSN 2663-2942 (Online).

journal homepage: http://chemistry.dnu.dp.ua
editorial e-mail: chem.dnu@gmail.com

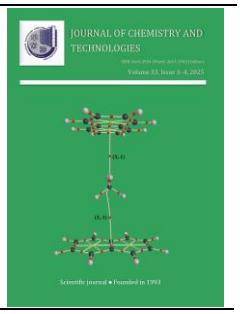

UDC 546.654.74

STUDY OF THE La-Ni-Ce TERNARY SYSTEM ACROSS THE $LaNi_5$-$CeNi_5$, $LaNi_5$-CeNi, AND LaNi-CeNi POLYTHERMAL SECTIONS

Ikhtiyar B. Bakhtiyarly[1], Elnara N. Ismayilova[1], Ziyafat M. Mukhtarova[1], Reyhan M. Agayeva[2], Faik M. Mammadov[1,2*]

[1]*Institute of Catalysis and Inorganic Chemistry of the Ministry of Science and Education of Azerbaijan, 113 H. Javid av., Baku Az1143, Azerbaijan*

[2]*Azerbaijan State Pedagogical University, Baku, AZ-1000 Azerbaijan*

Received 15 July 2025; accepted 25 September 2025; available online 25 December 2025

Abstract

Intermetallic compounds of transition metals, especially lanthanides, and the new phases based on them attract the attention of researchers as effective adsorbers for hydrogen. Using physicochemical analysis techniques, including Differential Thermal Analysis (DTA), Powder x-ray Diffraction (PXRD) and Scanning Electron Microscope (SEM), the ternary La-Ni-Ce system was investigated across the $LaNi_5$-$CeNi_5$, $LaNi_5$-CeNi, and LaNi-CeNi polythermal quasi-binary sections. The corresponding (T-x) phase diagrams have been constructed for the title system. The phase diagrams are quasi-binary and of the eutectic type. The systems have revealed wide regions of solid solutions based on starting compounds $LaNi_5$, LaNi, $CeNi_5$, CeNi. It has been established that the coordinates of the eutectic point formed on the basis of the initial components for the $LaNi_5$-$CeNi_5$, $LaNi_5$-CeNi, and LaNi-CeNi sections are 50 mol% $CeNi_5$, 1150 °C, 68 mol% CeNi, 650 °C, and 50 mol% CeNi, 620 °C, respectively. The obtained variable-composition phases can be considered as promising materials for hydrogen absorption.

Keywords: Transition metals; intermetallic compounds; $LaNi_5$; $CeNi_5$; solid solution; phase diagram.

ДОСЛІДЖЕННЯ ТРІКОМПОНЕНТНОЇ СИСТЕМИ La-Ni-Ce В ПОЛІТЕРМАЛЬНИХ РОЗРІЗАХ $LaNi_5$-$CeNi_5$, $LaNi_5$-CeNi ТА LaNi-CeNi

Іхтіяр Б. Бахтіарли[1], Ельнара Н. Ісмаїлова[1], Зіяфат М. Мухтарова[1], Рейхан М. Агаєва[2], Фаїк М. Мамедов[1*]

[1]*Інститут каталізу та неорганічної хімії Міністерства науки та освіти Азербайджану, вул. Г. Джавід, 113, Баку, Азербайджан, 1143*

[2]*Азербайджанський державний педагогічний університет, Баку, Азербайджан, 1000*

Анотація

Інтерметалідні сполуки перехідних металів, особливо лантаноїдів, та нові фази на їх основі привертають увагу дослідників як ефективні адсорбенти водню. За допомогою методів фізико-хімічного аналізу, включаючи диференційний термічний аналіз (ДТА), порошкову рентгенівську дифракцію (PXRD) та скануючу електронну мікроскопію (SEM), була досліджена трикомпонентна система La-Ni-Ce в політермальних квазібінарних ділянках $LaNi_5$-CeNi5, $LaNi_5$-CeNi та LaNi-CeNi. Для зазначеної системи побудовано відповідні фазові діаграми (Т-х). Фазові діаграми є квазібінарними та евтектичного типу. Системи виявили широкі області твердих розчинів на основі вихідних сполук $LaNi_5$, LaNi, $CeNi_5$, CeNi. Встановлено, що координати евтектичної точки, утвореної на основі вихідних компонентів для ділянок $LaNi_5$-$CeNi_5$, $LaNi_5$-CeNi та LaNi-CeNi, становлять відповідно 50 моль% $CeNi_5$, 1150 °C, 68 моль% CeNi, 650 °C та 50 моль% CeNi, 620 °C. Отримані фази зі змінним складом можна вважати перспективними матеріалами для адсорбції водню.

Ключові слова: перехідні метали; інтерметалічні сполуки; $LaNi_5$; $CeNi_5$; твердий розчин; фазова діаграма.

**Corresponding author: e*-mail: f.m.mammadov2017@gmail.com

doi: 10.15421/jchemtech.v33i4.335435

Journal of Chemistry and Technologies, 2025, *33*(4), 948-957

Introduction

Hydrogen energy is considered one of the most promising directions among alternative energy sources due to its ecological benefits, economic viability, and high energy density. For comparison, hydrogen has an energy density of 120.4 mc/kg, nearly three times higher than gasoline's energy density of 46 mc/kg [1–8].

Recent studies have focused on the metal alloys and intermetallic compounds of transition elements, especially lanthanides, highlighting their efficiency as hydrogen absorbers and their capability to produce high-purity hydrogen during desorption at relatively low temperatures [9–16]. Alloys within the Ln-Ni (Ln = La, Ce) system have been identified as highly promising for practical use in hydrogen adsorption and storage. Partial substitution of the metals in the intermetallic compounds $LaNi_5$ and $CeNi_5$ with other d- and f-transition elements has led to notable enhancements in the key properties required for efficient hydrogen accumulation and desorption [17–23]. Considering the role of phase diagrams in understanding the nature of phase equilibria, thermal stability and other technological parameters in the search for new materials [24–33], this article presents the results obtained from the study of polythermal sections $LaNi_5$-$CeNi_5$, $LaNi_5$-CeNi and LaNi-CeNi within the La-Ni-Ce ternary system.

Starting compounds. The initial components of the studied systems have been extensively investigated in several studies. It has been established that the compounds $LaNi_5$ and LaNi melt congruently at 1350 °C and 715 °C, respectively [34]. The $LaNi_5$ compound crystallizes in the hexagonal syngony (space group P6/mmm) with lattice parameters of a = 5.008 Å and c = 3.9830 Å [35]. LaNi, on the other hand, crystallizes in the orthorhombic syngony (space group Cmcm) with lattice parameters a = 3.9070 Å, b = 10.8100 Å, and c = 4.3960 Å [36].

The compounds $CeNi_5$ and CeNi melt congruently at 1340 °C and 700 °C, respectively [37]. The $CeNi_5$ compound crystallizes in the hexagonal syngony (space group P6/mmm) with lattice parameters a = 4.8600 Å and c = 3.9960 Å [38], while the CeNi compound crystallizes in the orthorhombic syngony (space group Cmcm) with lattice parameters a = 3.7880 Å, b = 10.5560 Å, and c = 4.3660 Å [36].

Experimental section

Synthesis. For the study, the compounds $LaNi_5$, $CeNi_5$, LaNi, and CeNi were synthesized in stoichiometric ratios from high-purity (h.p.) elements within evacuated graphitized quartz ampoules at a pressure of 10^{-3} Pa. The prepared ampoules were initially held at 400 °C for 12 hours, after which the temperature was gradually increased to 30–50 °C above the melting points of the initial components. To ensure the completion of the reaction between the elements, the alloys were mechanically stirred several times during the synthesis process. Subsequently, the resulting alloys were homogenized at 550 °C for 400 hours.

The individuality of the synthesized compounds was verified using differential thermal analysis (DTA) and X-ray phase analysis (XRD). The melting temperatures of the $LaNi_5$, $CeNi_5$, CeNi, and LaNi compounds were determined based on heating curves, and the results correspond to those reported in the literature [34–38].

Samples of the studied systems were prepared in stoichiometric ratios from binary compounds and synthesized in evacuated ampoules at temperatures 30 °C above the melting points of the initial components. The resulting alloys were thermally treated at 550 °C for 500 hours.

Research methods. The research was carried out using DTA and XRD techniques. DTA measurements were conducted on a NETZSCH STA 449 F3 device equipped with a platinum-platinum-rhodium thermocouple, over a temperature range from room temperature to approximately 1400 °C, at a heating rate of 10 K/min. The accuracy of the temperature measurements was ±2 K.

XRD analysis was conducted by capturing the powder diffraction patterns of the samples on a "D2 Phaser" diffractometer (Bruker, Germany) using CuKα radiation. The angular range was -50≤2θ≤80, with a scanning speed of 0.030–0.2 per minute.

The SEM analysis of some polished samples was performed using a TESCAN Vega 3 SBH scanning electron microscope.

Results and discussion

$LaNi_5$-$CeNi_5$ section. To investigate the $LaNi_5$-$CeNi_5$ section, 11 alloys with stoichiometric compositions were synthesized from the initial components (Table 1). The DTA results of the thermally treated samples indicate that the nature of chemical interactions in the system is relatively simple, and during heating, two endothermic effects characterizing the liquidus and solidus were observed in all alloys, except at

Journal of Chemistry and Technologies, 2025, *33*(4), 948-957

the eutectic point (e) at 50 mol.% $CeNi_5$ (Figure 2a).

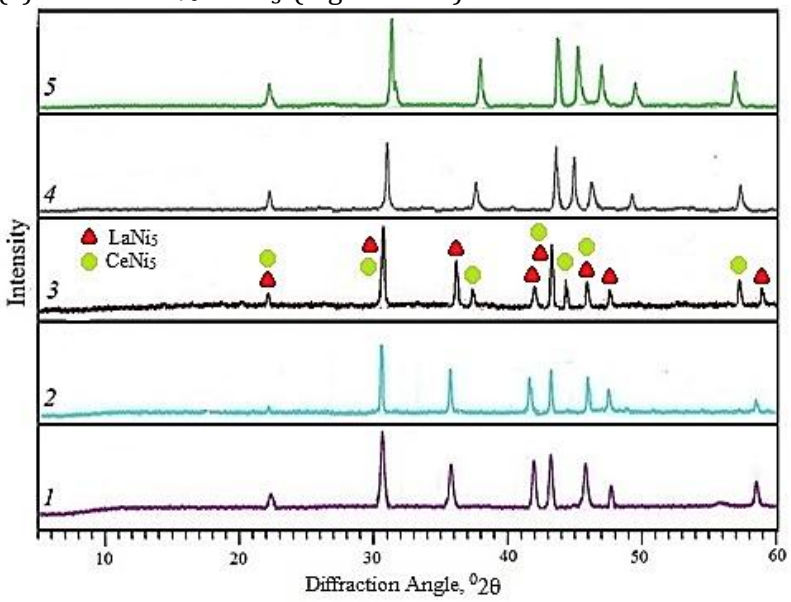

Fig. 1. Powder diffraction pattern of the alloy of the $LaNi_5$-$CeNi_5$ system. 1 – $LaNi_5$, 2 – 20 mol%$CeNi_5$, 3–40 mol%$CeNi_5$, 4 – 80 mol%$CeNi_5$, 5 – $CeNi_5$

The powder diffraction patterns of the thermally treated samples are shown in Figure 1. As seen in the figure, the diffraction pattern of the alloy with 50 mol% $CeNi_5$ consists of diffraction lines corresponding to $LaNi_5$ and $CeNi_5$ (α+α′), indicating a two-phase mixture. The diffraction patterns of alloys with 0÷20 and 80÷100 mol% $CeNi_5$ compositions exhibit diffraction features qualitatively identical to those of pure $LaNi_5$ and $CeNi_5$ compounds. This indicates the presence of extensive homogeneity regions based on these compounds. The dependence of lattice parameters on composition for selected alloys from the homogeneity region is shown in Figure 3a. As can be seen, this dependence exhibits a linear character according to Vegard's rule and is consistent with the corresponding phase diagram (Fig.3a).

Microstructure analysis has determined the solubility boundaries based on the $LaNi_5$ and $CeNi_5$ compounds. The solubility region is 29 mol% based on $LaNi_5$ and 35 mol% for $CeNi_5$. In the concentration range of 30–65 mol.%$CeNi_5$, the samples are two-phase.

Using the combined processing of DTA (Table 1, Figure 2a), XRD, and SEM analysis results, the phase diagram of the $LaNi_5$-$CeNi_5$ system was constructed (Figure 3b). The system is of a simple eutectic type and is characterized by the presence of extensive solid solution regions based on the initial components.

Table 1

Results of DTA for $LaNi_5$-$CeNi_5$ alloys

№	Composion, mol%		Temperature, ^{0}C
	$LaNi_5$	$CeNi_5$	
1	100	-	1350
2	90	10	1325; 1275
3	80	20	1275; 1225
4	70	30	1250; 1185
5	60	40	1200; 1150
6	50	50	1150
7	40	60	1200; 1165
8	30	70	1235; 1200
9	20	80	1275; 1225
10	10	90	1315; 1275
11	-	100	1340

The liquidus of the system consists of the primary crystallization curves of the α- and α'-phases. The system forms an eutectic based on both initial components, corresponding to a

Journal of Chemistry and Technologies, 2025, *33*(4), 948-957

composition of 50 mol% $CeNi_5$ and crystallizing at 1150 °C. At the eutectic temperature, the solubility region is 40 and 60 mol% $CeNi_5$. The homogeneity regions of the α- and α'-phases decrease as the temperature drops, and at room temperature, the solubility corresponds to 0–29 and 65–100 mol% $CeNi_5$, respectively.

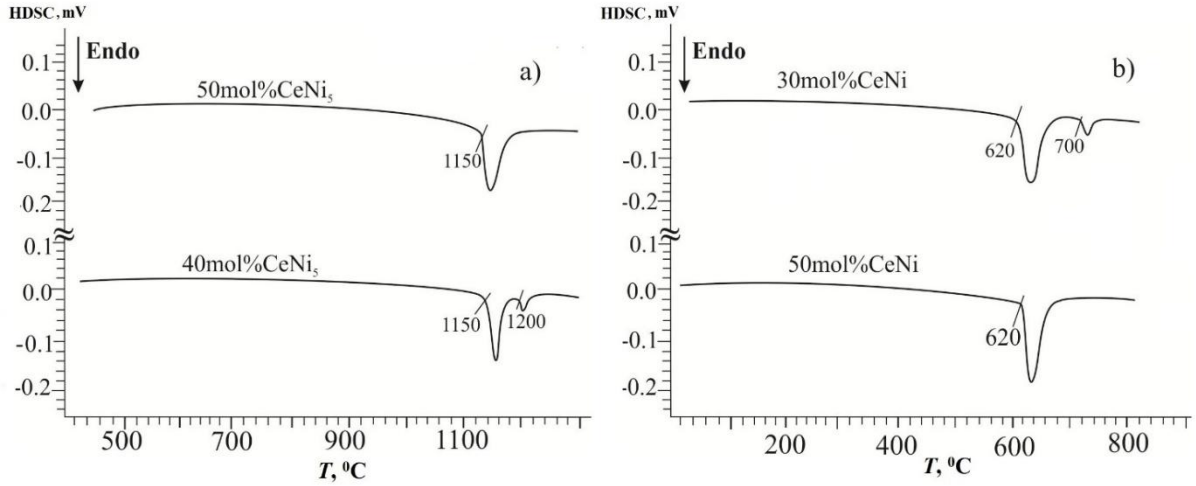

Fig. 2. Thermal curves of some alloys in the $LaNi_5$-$CeNi_5$(a) and LaNi-CeNi (b) sections

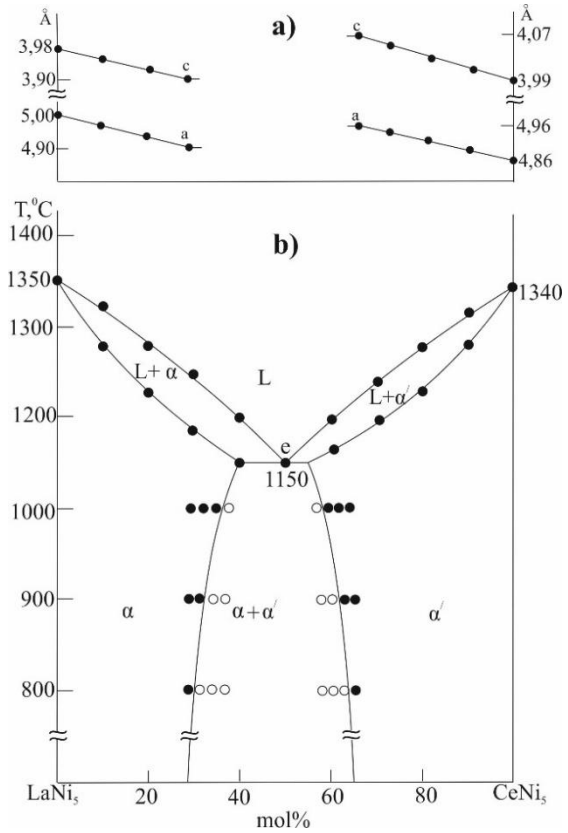

Fig. 3. Phase diagram of the $LaNi_5$-$CeNi_5$ section (b) and unit cell parameters versus composition for solid solutions (a)

It should be noted that, in order to determine the boundaries of the solubility region in the phase diagram depending on temperature, some compositions (Fig. 3b) were synthesized separately and thermally treated at 1000 °C, 900 °C, and 800 °C. After heat treatment at each temperature, the samples were quenched directly in ice water. The obtained samples were examined using SEM (Scanning Electron Microscopy) analysis (Fig. 4). As seen in the figure, the sample with 35 mol% $CeNi_5$ (Fig.4a) composition is single-phase, while the sample with 37 mol% $CeNi_5$ (Fig.4b) composition is two-phase at room temperature.

Similarly, in other systems studied, the boundaries of the solid solution regions

Journal of Chemistry and Technologies, 2025, *33*(4), 948-957

depending on temperature were determined using the same method.

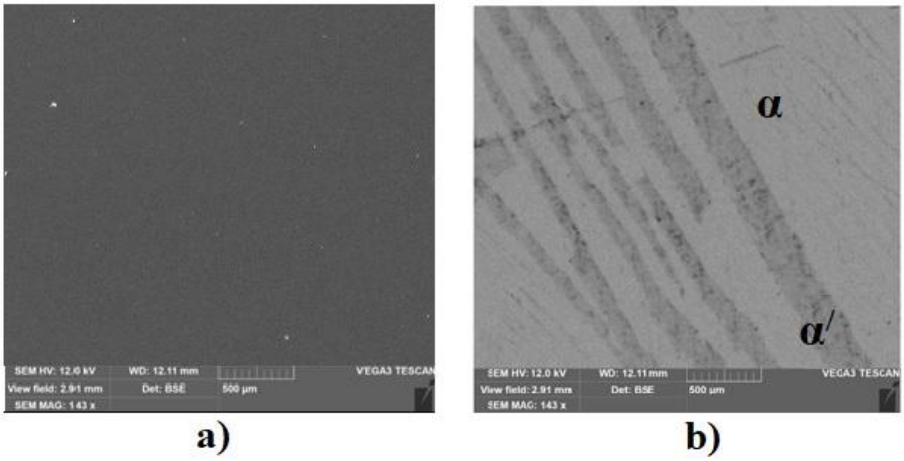

Fig. 4. SEM images of the samples containing 35 mol%$CeNi_5$ (a) and 37 mol% $CeNi_5$ (b) in the $LaNi_5$-$CeNi_5$ system

$LaNi_5$-CeNi section. To investigate DTA, alloys with compositions of 10, 20, 30, 40, 50, 60, 70, 80, and 90 mol% CeNi were synthesized (Table 2). Thermograms of the equilibrated alloys were recorded, and two effects were observed in the samples (except for 68 mol% CeNi). One of these thermal effects characterizes the liquidus temperature, while the other corresponds to the solidus temperature.

Table 2

Results of DTA for $LaNi_5$-CeNi alloys

№	Composions, mol%		Temperature, ^{0}C
	$LaNi_5$	CeNi	
1	100	-	1350
2	90	10	1325; 1245
3	80	20	1285; 825
4	70	30	1250; 675
5	60	40	1200; 650
6	50	50	850; 650
7	40	60	740; 650
8	30	70	650
9	20	80	675; 650
10	10	90	690; 665
11	-	100	700

XRD analysis reveals that the diffraction patterns of samples with 15 and 95 mol% CeNi are identical to the diffraction patterns of the initial components (Figure 5). As seen in the figure, a wide solubility region is observed for both initial components. The diffraction pattern of the powder diffractogram of alloys with >20 mol% CeNi aligns with that of the $LaNi_5$ compound. The diffraction patterns of samples with 10–80 mol% $LaNi_5$ compositions consist of a mixture of the diffraction patterns of the initial components, further proving that no new phase forms in the section. Using the TOPAS V3.0 software, the lattice parameters of some samples from the solid solution region were calculated based on their powder diffraction patterns (Figure 6a). As illustrated in the figure, this dependence displays a linear behavior.

Journal of Chemistry and Technologies, 2025, *33*(4), 948-957

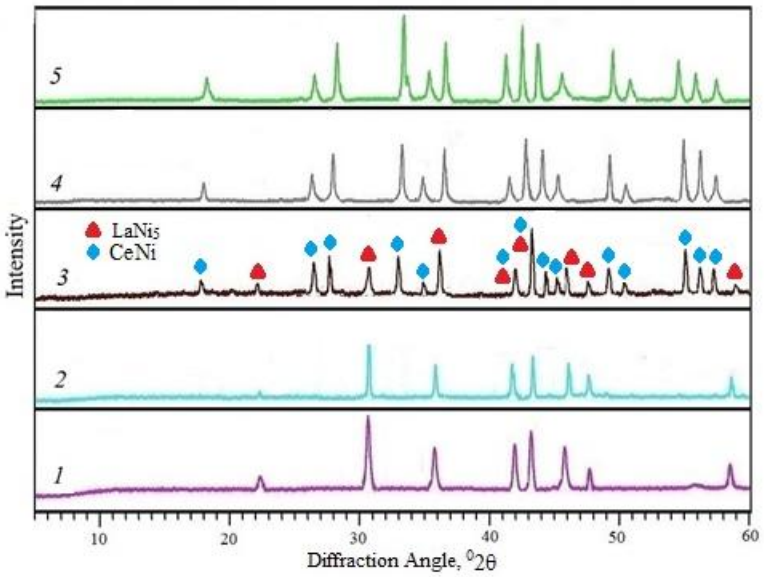

Fig. 5. Powder diffraction pattern of the alloy of the $LaNi_5$-CeNi system. 1 – $LaNi_5$, 2 – 15mol% CeNi, 3 – 50mol% CeNi, 4 – 95 mol% CeNi, 5 – CeNi

The phase diagram of the $LaNi_5$-CeNi system was constructed using data from DTA, XRD, and SEM analyses (Figure 6b). The liquidus of the system consists of two curves characterizing the primary crystallization of solid solutions based on $LaNi_5$ (α) and CeNi (β). The system is quasi-binary and belongs to the eutectic type. The eutectic has a composition of 68 mol% CeNi and crystallizes at 650 °C. The solubility based on the initial components is maximal at the eutectic temperature (650 °C), reaching 30 mol% CeNi and 18 mol% $LaNi_5$, respectively. SEM indicates that alloys with 0–20 mol% and 92–100 mol% CeNi compositions are single-phase (Fig.7a), whereas alloys with 20–92 mol% CeNi compositions are two-phase (Fig.7b). In the subsolidus region, all alloys in the composition range of 35–85 mol% CeNi consist of two-phase (α and β/) mixtures.

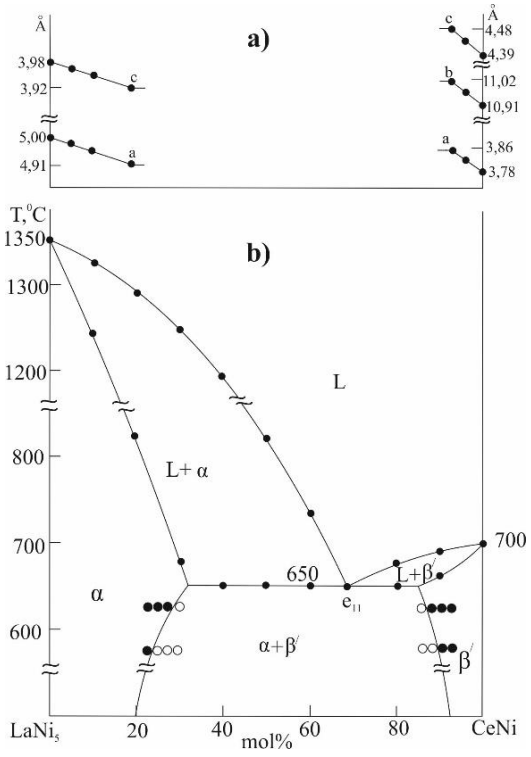

Fig. 6. Phase diagram of the $LaNi_5$-CeNi section (b) and unit cell parameters versus composition for solid solutions (a)

Journal of Chemistry and Technologies, 2025, *33*(4), 948-957

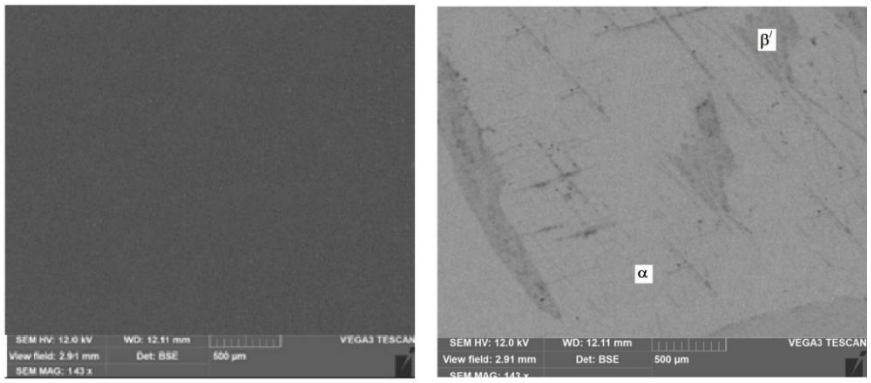

Fig. 7. SEM images of the samples containing 22 mol%CeNi (a) and 24 mol%CeNi (b) in the $LaNi_5$-CeNi system

In the LaNi-CeNi section, 11 alloys (Table 3) were synthesized under optimal synthesis conditions and homogenized at 550 °C for approximately 500 hours. Thermograms recorded for DTA revealed two endothermic effects. Only the sample with 50 mol% CeNi composition exhibited a single thermal effect at 620 °C, which characterizes the eutectic equilibrium (e) (Fig. 2b).

Table 3

Results of DTA for LaNi-CeNi alloys

№	Composions, mol%		Temperature, ^{0}C
	LaNi	CeNi	
1	100	-	715
2	90	10	710; 660
3	80	20	705; 630
4	70	30	700; 620
5	60	40	765; 620
6	50	50	620
7	40	60	665; 620
8	30	70	675; 620
9	20	80	685; 640
10	10	90	695; 660
11	-	100	700

To precisely determine the boundaries of the solid solution regions in the system based on the initial components, several samples with specific compositions (10 and 15 mol% for LaNi, and 80 and 85 mol% for CeNi) were resynthesized. Similary, in this system, the parameters of the unit cell are linear depending on the composition of solid solutions (Fig. 8a).

The phase diagram of the LaNi-CeNi section was constructed (Fig. 8b) using data from DTA (Table 3 and Fig. 2b), XRD, and SEM analyses.

The system was identified as quasi-binary, with the phase diagram classified as eutectic in nature. The liquidus of the system consists of two curves corresponding to the primary crystallization of LaNi and CeNi. The boundaries of the β and β/ solid solutions observed based on both components have been refined with SEM analysis (Fig.9). For example, as illustrated in figure 9, the sample with 10 mol% CeNi composition (Fig.9a) exhibits a single-phase structure, whereas the sample with 12 mol% CeNi composition (Fig.9b) displays a two-phase structure. In the system, 12 mol% CeNi dissolves in LaNi, while 20 mol% LaNi dissolves in CeNi. In the subsolidus region, joint crystallization of the LaNi and CeNi phases occurs within the concentration range of 12 mol% to 80 mol% CeNi. The coordinates of the eutectic are 50 mol% LaNi, with a temperature of 620 °C.

Journal of Chemistry and Technologies, 2025, *33*(4), 948-957

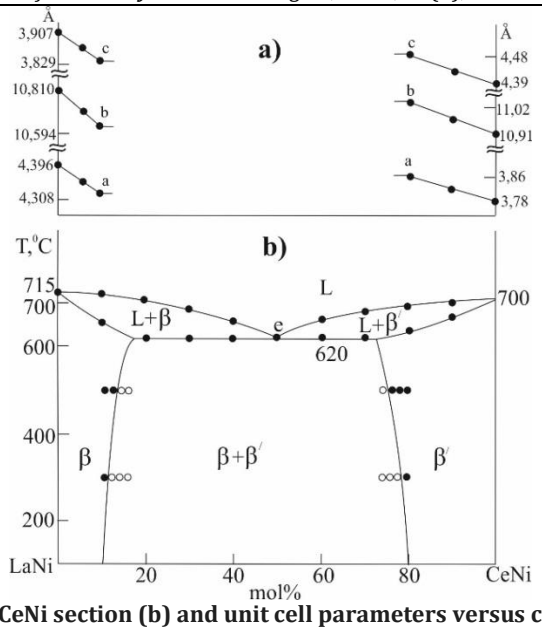

Fig. 8. Phase diagram of the LaNi-CeNi section (b) and unit cell parameters versus composition for solid solutions (a)

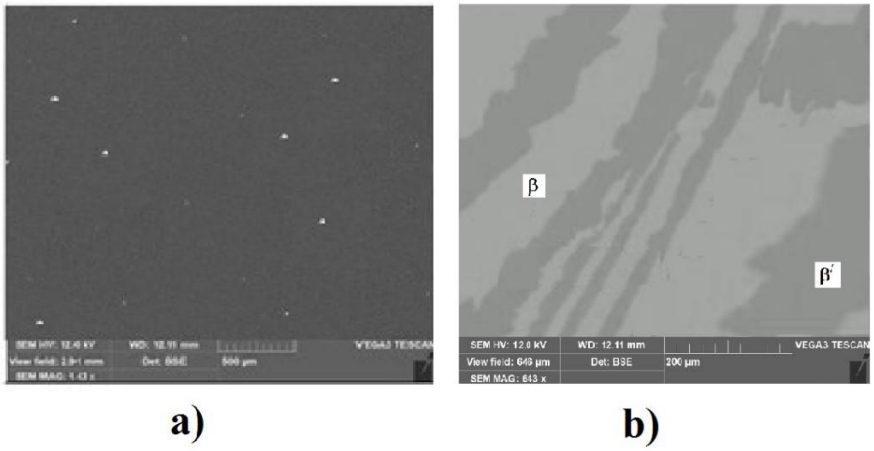

Fig. 9. SEM images of the samples containing 10 mol% CeNi (a) and 12 mol% CeNi (b) in the LaNi-CeNi system

Conclusion

Thus, the aforementioned sections of the La-Ni-Ce ternary system were investigated using physicochemical analysis methods, and their phase diagrams were constructed. It has been determined that all three systems are quasi-binary and are characterized by the formation of limited solubility regions based on the initial components. The coordinates of the eutectic formed based on the initial components for the $LaNi_5$-$CeNi_5$, $LaNi_5$-CeNi, and LaNi-CeNi sections are, 50 mol% $CeNi_5$ at 1150 °C, 68 mol% CeNi at 650 °C, and 50 mol% CeNi, respectively, at 620 °C. The studied systems are characterized by the formation of solid solution regions based on the initial compounds. Thus, at a temperature of 300 K, the solubility ranges are 29 and 35 mol% in the $LaNi_5$-$CeNi_5$ system, 20 and 8 mol% in the $LaNi_5$-CeNi system and 12 and 20 mol% in the LaNi-CeNi system, based on the initial components, respectively. The phase diagrams examined in the system represent a theoretical approach to determining the initial technological parameters of the corresponding materials. The properties of the resulting materials can be optimized by changing the composition of the resulting solid solutions.

Conflicts of Interest

The authors declare no conflict of interest.

References

[1] Molinas, B., Pontarollo, A., Scapi, M., Peretti, H., Melnichu, M., Corso, H., Auror, A., Mirabile D., Montone, A. (2016). The optimization of $MmNi_{5-x}Al_x$ hydrogen storage alloy for sea or lagoon navigation and transportation. *Int. J. Hydrog. Energy. 41*(32), 14484–14490. https://doi.org/10.1016/j.ijhydene.2016.05.222

[2] Srivastava, S., Panwar, K. (2015). Effect of transition metals on ball-milled $MmNi_5$ hydrogen storage alloy.

Mater. Renew. Sustain. Energy. 4(19), 1–10. https://doi.org/10.1007/s40243-015-0062-9

[3] Kulova, T. L., Nikolayev, I. I., Fateyev, V.N., Aliyev, A. Sh. (2018). Modern electrochemical systems of energy accumulation. *Chem. Problems. 16*(1), 9–34. https://doi.org/10.32737/2221-8688-2018-1-9-34

[4] Todorovic, R. (2015). Hydrogen Storage Technologies for Transportation Application. *J. Undergraduate Research*. *8*(1), 56–59. https://doi.org/10.5210/jur.v8i1.7541

[5] Kurc, B., Gross, X., Szymlet, N., Rymaniak, Ł., Wozniak, K., Pigłowska, M. (2024). Hydrogen-powered vehicles: a paradigm shift in sustainable transportation. *Energies*, *17*(69), 4768. https://doi.org/10.3390/en17194768

[6] Barthelemy, H., Weber, M., Barbier, F. (2017). Hydrogen storage: Recent improvements and industrial perspectives. *Int. J. Hydrogen Energy, 42*(11), 7254–7262. https://doi.org/10.1016/j.ijhydene.2016.03.178

[7] Talaganis, B.A. Esquivel, M.R. Meyer, G. (2009). Atwo-stage hydrogen compressor based on (La, Ce, Nd, Pr)Ni_5 intermetallics obtained by lowen ergyme chanical alloying–low temperature annealing treatment. *Int. J. Hydrogen Energy, 34*, 2062–2068. https://doi.org/10.1016/j.ijhydene.2008.11.052

[8] Ngameni, R. Mbemba, N. Grigoriev, S. A., Millet, P. (2011). Comparative analysis of the hydriding kinetics of $LaNi_5$, $La_{0.8}Nd_{0.2}Ni_5$ and $La_{0.7}Ce_{0.3}Ni_5$ compounds. *Int. J. Hydrogen Energy, 36*(6), 4178–4184. https://doi.org/10.1016/j.ijhydene.2010.06.107

[9] Lototskyy, M.V., Yartys, V.A. Pollet, B.G., Jr Bowman, R. C. (2014). Metal hydride hydrogen compressors: A review. *Int. J. Hydrog Energy, 39*(11), 5818–5851. https://doi.org/10.1016/j.ijhydene.2014.01.158

[10] Gahleitner, G. (2013). Hydrogen from renewable electricity: an international review of power-to-gas pilot plants for stationary applications. *Int. J. Hydrog Energy, 38*(5), 2039–2061. https://doi.org/10.1016/j.ijhydene.2012.12.010

[11] An, X.H., Gu, Q.F., Zhang, J.Y., Chena, S.L., Yu, X.B., Li, Q. (2013). Experimental investigation and thermodynamic reassessment of La–Ni and $LaNi_5$–H systems. *Calphad*, *40*, 48–55. https://doi.org/10.1016/j.calphad.2012.12.002

[12] Afshari, M. (2017). Structural and magnetic properties of $LaNi_5$ and $LaNi_{3.94}Al_{1.06}$ alloys, before and after hydrogenation. *J. Supercond. Nov. Magn*,*30* (8),2255–2259. https://doi.org/10.1007/s10948-017-4045-1

[13] Sato, T., Saitoh, H., Utsumi, R., Ito, J., Nakahira, Y., Obana, K., Takagi, S., Orimo, S. (2023). Hydrogen Absorption Reactions of Hydrogen Storage Alloy $LaNi_5$ under High Pressure. *Molecules, 28*, 1256. https://doi.org/10.3390/molecules28031256

[14] Mardani, M., Bajenova, I., Khvan, A., Cheverikin, V., Richter, K. (2020). Phase transformations and phase equilibria in the LaeNi and LaeNieFe systems. Part 1: Liquidus & solidus projections. *J. Alloys and Compd. 845*(10), 156356. DOI:10.1016/j.jallcom.2020.156356

[15] Joubert, J.-M., Paul-Boncour, V., Cuevas, F., Zhang, J., Latroche, M. (2021). $LaNi_5$ Related AB_5 Compounds: Structure, Properties and Applications. *J. Alloys Compd*. 862, 158163. https://doi.org/10.1016/j.jallcom.2020.158163.

[16] Zareii, S. M., Arabi, H., Pourarian, F. (2014). A comprehensive investigation of structural, morphological, hydrogen absorption and magnetic properties of $MmNi_{4.22}Co_{0.48}Mn_{0.15}Al_{0.15}$ alloy. *Int. J. Mod. Phys. B, 28*(19), 1450125. https://doi.org/10.1142/S0217979214501252

[17] Zhang, L., Allendorf, M.D., Balderas–Xicohténcatl, R., Broom, D.P., Fanourgakis, G.S., Froudakis, G.E. (2022). Fundamentals of Hydrogen Storage in Nanoporous Materials. *Prog. Energy*., *4*(4), 042013. doi:10.1088/2516-1083/ac8d44

[18] Shashikala, K. (2012). *15-Hydrogen storage materials. İn book, Functional materials*. London: Elsevier. https://doi.org/10.1016/B978-0-12-385142-0.00015-5

[19] Liu, Y., Chabane, D., Elkedim, O. (2024). Optimization of $LaNi_5$ hydrogen storage properties by the combination of mechanical alloying and element substitution. Int. *J. Hydrogen Energy*. *53*(69), 394–402. doi:10.1016/j.ijhydene.2023.12.038

[20] Wen, X., Wang, B., Li, C., Liu, T. (2024). Effect of La doping on the structural stability and hydrogen adsorption behavior of Ce-La alloys. *J. Alloys Compd*. *982*, 173553. https://doi.org/10.1016/j.jallcom.2024.173553

[21] Jain, R.K., Jain, A., Agarwal, Sh. N., Lalla, P., Ganesan, V., Phase, D.M., Jain, I.P. (2007). Hydrogenation behaviour of Ce-based AB_5 intermetallic compounds. *J. Alloys Compd., 440*, 84–88. https://doi.org/10.1016/j.jallcom.2006.08.326

[22] Borzone, E. M., Baruj, A., Blanco, M.V., Meyer, G.O. (2013). Dynamic measurements of hydrogen reaction with $LaNi_{5-x}Sn_x$ alloys. *Int. J. Hydrogen Energy, 38*(18), 7335–7343. https://doi.org/10.1016/j.ijhydene.2013.04.035

[23] Jain, R.K., Jain, A., Agarwa Sh., Lalla, N.P., Ganesan, V., Phase, D.M., Jain, I.P. (2007). Characterization and hydrogenation of $CeN_{5-x}Cr_x$ (x=0, 1, 2) alloys. *J. Alloys Compd*., *430*, 165–169. https://doi.org/10.1016/j.jallcom.2006.05.013

[24] Bakhtiyarli, I.B, Mammadov, V.S, Mukhtarova, Z.M, Abdullayeva, A.S (2023). Phase Equilibrium In The Quasi-Ternary System Y_2O_2S–Ga_2S_3–Tb_2O_2S. *Azerb. Chem. Journal, 1*, 55–64.

[25] Mammadov, F. M. (2021). New version of the phase diagram of the MnTe-Ga_2Te_3 system. *New Materials, Compounds and Applications*, *5*(2), 116–121.

[26] Mammadov, F.M., Babanly, D.M., Orujlu, E.N., Niftiyev, N.N., Salmanov, F.T., Gasimov, R. J., Bayramov, M.A., Amiraslanov, I. R., Babanly, M. B. (2025). The phase equilibria in the MnSe–Ga_2Se_3–In_2Se_3 system, crystal structure and some physical properties of $MnGaInSe_4$. *J. Alloys Compd*., *1036*, 181814. https://doi.org/10.1016/j.jallcom.2025.181814

[27] Mammadov, Sh.H., Ismailova, R. A., Gasanova, M. B. (2025). Ag_2S-Ga_2S_3-PbS quasi-ternary system. Journal of chemistry and technologies. *33*(2), 1-7.

[28] Ismayilova, E.N., Baladzhayeva, A.N., Mashadiyeva, L.F. (2021). Phase equilibria along the Cu_3SbSe_4-$GeSe_2$ section of the Cu-Ge-Sb-Se system. *New Materials, Compounds and Applications*, *5*(1), 52–58.

[29] Aghazade, A. I., Orujlu, E. N., Salimov, Z. E., Mammadov, A. N., Babanly, M. B. (2023). Experimental investigation of the solid phase equilibria at 300 K in the $SnBi_2Te_4$-$PbBi_2Te_4$-Bi_2Te_3 system. *Phys. Chem. Solid State*, *24*(3), 453–459. https://doi.org/10.15330/pcss.24.3.453-459

[30] Mammadov, F.M. (2020). FeS-$FeGa_2S_4$-$FeGaInS_4$ system. *Chem. Problems, 2*(18), 214–221.

https://doi.org/10.32737/2221-8688-2020-2-214-221

[31] Ismailova, E. N. Mashadieva, L. F., Bakhtiyarly, I. B., Gasymov, V. A., Gurbanova, R. J., Mammadova, F. M. (2025). Phase Equilibria In The Cu_2Se - Cu_3SbSe_4 - Cu_2SnSe_3 System. *Chem. Problems*, *1*(23), 36–46. https://doi.org/10.32737/2221-8688-2025-1-36-46

[32] Zhang, D., Jinke, T., Gschneidner, K. A. (1991). Are determination of the La–Ni phase diagram from LaNi to $LaNi_5$ (50–83.3 at%Ni). *J. Less- Common Met., 169*, 45–53. https://doi.org/10.1016/0022-5088(91)90234-U

[33] Inui, H., Yamamoto, T., Zhang, D., Yamaguchi, M. (1999). Microstructures and defect structures in intermetallic compounds in the La–Ni alloy system. *J. Alloys Compd.*, *293*, 140–145. https://doi.org/10.1016/S0925-8388(99)00314-X

[34] An, X.H., Gu, Q.F., Zhang, J.Y., Chen, S.L., Yu, X.B., Li, Q. (2013). Experimental investigation and thermodynamic reassessment of La-Ni and $LaNi_5$–H systems. *Calphad, 40,* 48–55. https://doi.org/10.1016/j.calphad.2012.12.002

[35] Okamoto, H. (2020). Supplemental literature review of binary phase diagrams: Al-Pt, As-U, C-Li, C-Mg, Cd-Nd, Co-Ta, Fe-Re, Ga-Y, La-Ni, O-V, P-Si, and Re-Zr. *J. Phase Equilib. Diffus*. *41*, 722–733. https://doi.org/10.1007/s11669-020-00839-9

[36] Dwight, A.E., Conner, Jr, R.A., Downey, J.W. (1965). Equiatomic compounds of the transition and lanthanide elements with Rh, Ir, Ni and Pt. *Acta Crystallogr., 18* (5), 835–839. https://doi.org/10.1107/S0365110X65002050

[37] Xiong, W. Du, Y. Lu, X. Schuster, J., Chen, H. (2007). Reassessment of the Ce-Ni binary system supported by key experiments and ab initio calculations. *Intermetallics, 15*(11), 1401–1408. https://doi.org/10.1016/j.intermet.2007.04.004

[38] Pourarian, F., Wallace, W.E. (1982). Hydrogen storage in $CeNi_{5-x}Cu_x$. *Less-Common Metals, 87*(2), 275–281. https://doi.org/10.1016/0022-5088(82)90094-7